Published as Materials Science and Engineering: A, 700, 2017, Pages 312-320, doi.org/10.1016/j.msea.2017.05.115.

Evolution of microstructure and mechanical properties of an as-cast Mg-8.2Gd-3.8Y-1.0Zn-0.4Zr alloy processed by high pressure torsion

W.T. Sun[1], C. Xu[2], X.G. Qiao[1], M.Y. Zheng[1]*, S. Kamado[2], N. Gao[3], M.J. Starink[3]

[1] School of Materials Science and Engineering, Harbin Institute of Technology, Harbin 150001, PR China

[2] Department of Mechanical Engineering, Nagaoka University of Technology, Nagaoka 940-2188, Japan

[3] Materials Research Group, Faculty of Engineering and the Environment, University of Southampton, Southampton SO17 1BJ, UK

* zhenghe@hit.edu.cn, Tel.: +86 451 86402291, fax: +86 451 86413922

Abstract:

The novel Mg-8.2Gd-3.8Y-1.0Zn-0.4Zr alloy with high content of rare earth elements has been processed successfully by high pressure torsion (HPT) starting from an as-cast condition. HPT processing was conducted at room temperature for a range of turns from 1/8 to 16, and the evolutions of microstructure and microhardness were investigated. The average grain size decreases from ~85 μm in the as-cast condition to ~55 nm when the equivalent strain reaches ~6.0, and remains almost constant on further strain increase. Meanwhile, the coarse netlike $Mg_3(Gd,Y)$ second phase structures are gradually broken into fine dispersed particles and the dislocation density increases. The microhardness of the alloy increases with increasing strain, and when the equivalent strain reaches ~6.0, the microhardness reaches a saturated value of about 115 HV, which is higher than that obtained by conventional extrusion / rolling of this alloy. The full range of possible mechanisms of hardening are analysed and this reveals that hardening is primarily due to the pronounced grain refinement, which is substantially

stronger than that for HPT-processed conventional Mg alloys, and to the homogeneously distributed fine second phase particles and the high dislocation density.

Key words: Mg-RE alloy; High pressure torsion; Microstructure; Mechanical properties

1. Introduction

Magnesium alloys are attractive candidate materials for use in lightweight structures in automotive and aerospace industries due to their low density, and good specific strength and stiffness [1]. Unfortunately, some of the properties of conventional Mg alloys, such as strength, ductility and thermal stability, are inferior to those of competitor light alloys, which restrict their application. Following the development of an ultra-high strength Mg-2Y-1Zn (at%) alloy by rapidly solidified powder metallurgy (RS P/M) processing [2], Mg-RE-Zn (where RE represents rare earth elements) alloys exhibiting superior mechanical properties at both room and elevated temperatures have drawn considerable interest. Due to the presence of RE elements and Zn, these alloys contain long-period stacking ordered (LPSO) structures [3, 4].

Grain refinement is an effective approach to improve strength of metals whilst retaining reasonable ductility [5]. It is generally impossible to achieve a nanostructured alloy by conventional thermomechanical processing because of the geometrical limitation on the amount of strain imposed on the materials [6]. High pressure torsion (HPT) as a typical severe plastic deformation (SPD) process to fabricate bulk ultrafine-grained and nanocrystalline metallic materials has attracted wide attention. During HPT, an extremely large torsional strain and high hydrostatic pressure of several GPa are

simultaneously imposed on the material [7]. HPT has the potential for achieving greater grain refinement than other SPD procedures. Application of quasihydrostatic pressure in HPT prevents cracking, so HPT can be used to deform Mg alloys at low temperature to produce bulk ultrafine-grained Mg alloys [8, 9]. However, a full analysis of strengthening mechanisms, e.g. addressing the effects of grain boundary strengthening, dislocation strengthening, solute strengthening and dispersion strengthening, in the novel Mg alloys with very high content of rare earth elements (>10 wt%) has been limited.

It has been found that the microstructure of pure Mg, processed by extrusion followed by HPT for 8 turns at room temperature, is more homogenous than that of the as-cast counterpart, with grain sizes around ~1.0 μm and a hardness of ~52 HV [10]. In contrast, for Mg alloys, a more significant grain refinement can be obtained by HPT. For example, a uniform microstructure with a grain size of 150 nm and microhardness of 990 MPa were obtained in Mg-1Zn-0.13Ca (wt%) after HPT for 5 turns [11]. The ultrafine-grained structure in HPT-processed Mg-9.33Gd (wt%) is very stable, with grain sizes remaining about 100 nm during isochronal annealing up to 300 ^{o}C [12]. An extruded Mg-9Gd-4Y-0.4Zr (wt%) alloy with an initial grain size of ~8.6 μm was refined to ~85 nm through HPT for 16 turns, and the HPT processed alloy exhibited superplastic behavior with a maximum strain rate sensitivity of ~0.51 at 350 ^{o}C [13]. A partially nanocrocrystalline structure with a grain size of 20-30 nm was formed in the Mg-4.7Y-4.6Gd-0.3Zr (wt%) alloy after HPT processing at room temperature, while a grain size of 60-90 nm was achieved through HPT processing at 200 ^{o}C [14].

In previous studies, ultrahigh strength and fair ductility have been achieved in the LPSO-containing Mg-8.2Gd-3.8Y-1.0Zn-0.4Zr alloy by conventional extrusion / rolling and ageing treatment [15, 16]. In the present research, the as-cast Mg-8.2Gd-3.8Y-1.0Zn-0.4Zr alloy was processed by HPT at ambient temperature, and the evolutions of microstructure and hardness of the alloy during HPT were studied. The aim is to investigate whether HPT can refine the microstructure and improve the properties of a cast Mg alloy with very high RE content beyond what is achieved by conventional processing, and to study the range of strengthening mechanisms induced by HPT, including grain refinement, dislocation generation and refinement of RE containing second phase structures.

2. Experimental procedures

The starting material used in the present study was a Mg-8.2Gd-3.8Y-1.0Zn-0.4Zr (wt%) alloy produced by direct-chill casting [17]. To obtain samples for HPT processing, disks with a diameter of 10.0 mm and a thickness of 1.0 mm were machined from the as-cast ingot. These disks were ground with abrasive papers on both sides to a final thickness of ~0.85 mm and subsequently processed by HPT with 1/8, 1/4, 1/2, 1, 2, 5, 10 and 16 turns. All HPT processing was performed at ambient temperature under quasi-constrained conditions applying an imposed pressure of 6.0 GPa and a rotational speed of 1 rpm. The microstructures of HPT-processed samples at selected positions were observed using an Olympus D11 optical microscope (OM), a JEOL JSM-7000F field-emission scanning electron microscope (FE-SEM), and an FEI TECNAI G^2 F30 transmission electron microscope (TEM) operated at 200 kV accelerating voltage. To

reveal the grain boundaries, the samples for OM observation were chemically etched in a solution of 6 g picric acid, 5 ml acetic acid, 10 ml distilled water and 100 ml ethanol. For TEM observations, thin disks with a diameter of 3 mm were punched out from the HPT-processed disks, where the centres of these smaller disks were at 2.5 mm distance from the centres of the HPT-processed disks. These 3 mm disks were mechanically ground to ~50 μm in thickness and further ion-milled by a Gatan plasma ion polisher with an incidence angle of 15°. The average grain sizes of HPT-processed samples were determined from TEM images using the modified line intercept method [18], and the grain size D was taken as D=1.455$\bar{L}$, where $\bar{L}$ is the average line intercept [19, 20]. The constituent phases of as-cast and HPT-processed samples were measured by an X'Pert PRO X-ray diffractometer. The crystallite size and microstrain of the HPT-processed samples were determined by analyzing the X-ray diffractometry (XRD) patterns via the Materials Analysis Using Diffraction (MAUD) software [21, 22]. A detailed description of this analysis was provided previously in references [20, 23]. The dislocation density ρ was deduced from the measured microstrains $\langle\varepsilon^2\rangle^{1/2}$ using [20, 24, 25]:

$$\rho = \frac{2\sqrt{3}\langle\varepsilon^2\rangle^{1/2}}{D_c b} \quad (1),$$

where b is the Burgers vector and D_c is the crystallite size.

Vickers hardness was measured along the diameters of the disks with incremental steps of 0.5 mm using a Zwick microhardness tester under a constant load of 500 g and a dwell time of 15 s. Each reported Vickers microhardness value is determined by averaging values for three indentations at positions that are equidistant to the centre of

the disk. In order to avoid any interference between the strain fields of individual indentations, the distance between adjacent indentation centres is selected to be about 0.3 mm, which is approximately three times the size of indentations.

3. Results and analysis

3.1 Microstructure evolution after HPT processing

Fig.1 shows the microstructure of the as-cast Mg-8.2Gd-3.8Y-1.0Zn-0.4Zr alloy. The microstructure mostly consists of α-Mg grains of size of ~85 μm surrounded by Mg_3(Gd,Y) eutectic compounds. In addition, a small amount of lamellar LPSO phases are observed around the intermetallic Mg_3(Gd,Y) compounds, as shown in Fig.1b, which is consistent with our previous studies [3, 17].

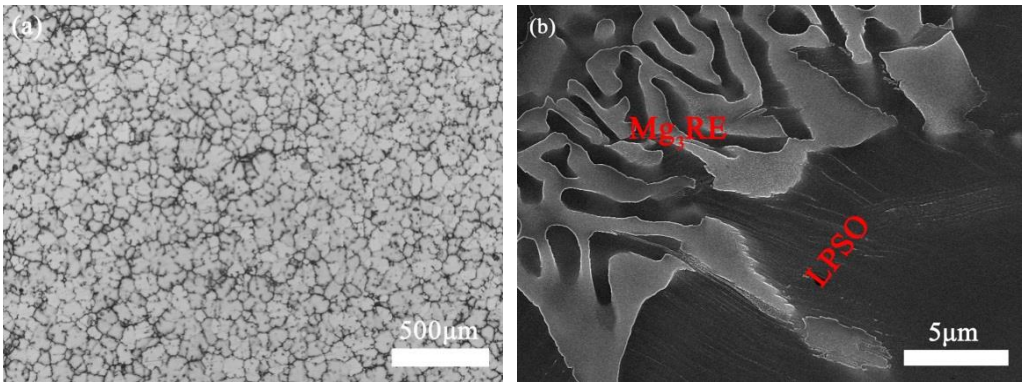

Fig.1 (a) Optical and (b) SEM micrographs of the as-cast Mg-8.2Gd-3.8Y-1.0Zn-0.4Zr alloy.

Optical microscopy reveals that the microstructures across the sample diameter undergo substantial changes during HPT processing, as shown in Fig.2. The average grain size in the central region is relatively large and remains almost unchanged up to 5 turns. After HPT processing for 10 turns and 16 turns, microstructure refinement occurs in the central region. On the other hand, in periphery regions the microstructure is refined from the first turn. After HPT deformation for 2 turns, the original grain

boundaries at the edge of the samples are not discernable by optical microscopy, which is ascribed to a very small size of new grains caused by high strains and the presence of refined intermetallic particles. The microstructure evolution at half-radius regions exhibits a similar trend as at the edges. After 10 turns, homogeneous microstructures are observed at both the half-radius and the edge of the disk. On further increase of strain, the microstructures at these positions show little change and remain homogeneous.

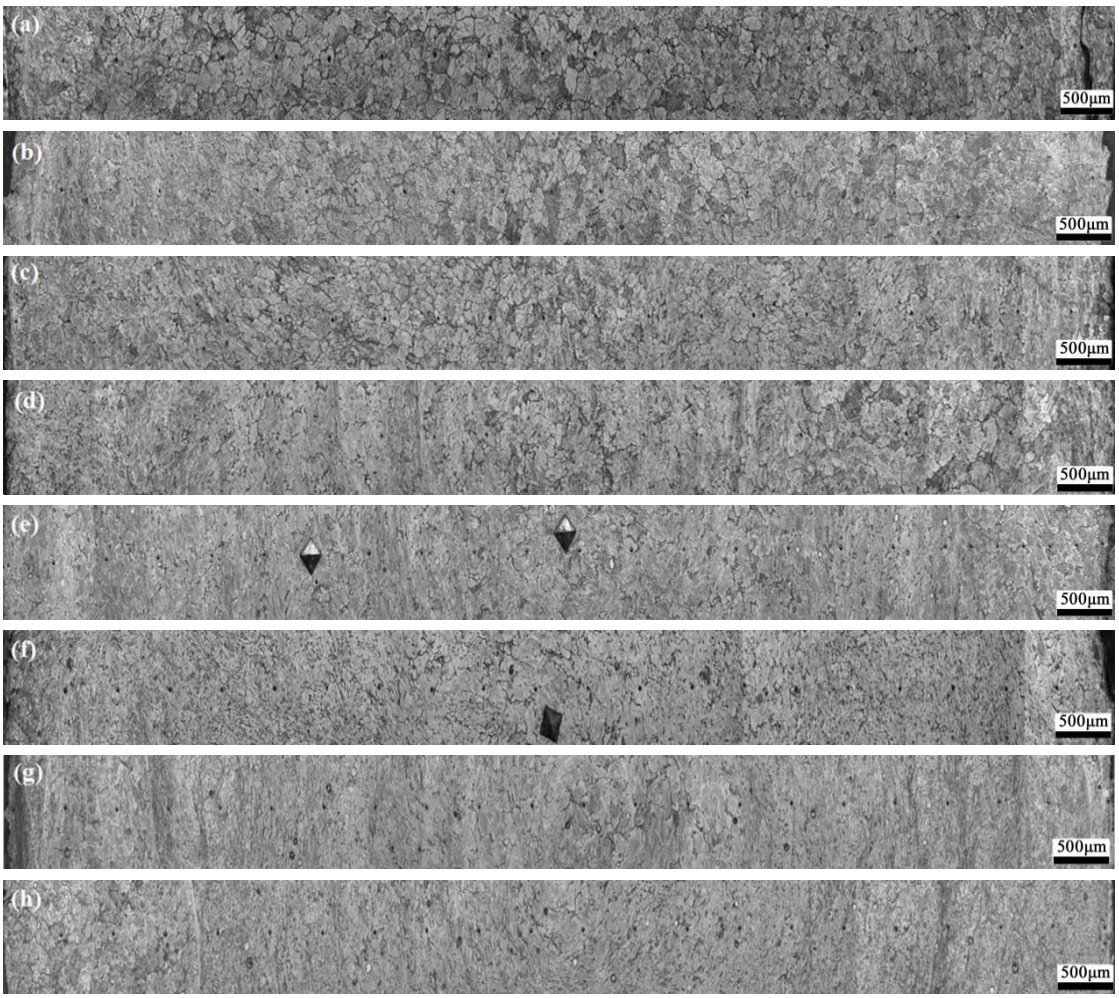

Fig.2 Optical micrographs showing the microstructures across the diameter on the surfaces of Mg-Gd-Y-Zn-Zr disks processed by HPT at room temperature for (a) HPT1/8; (b) HPT1/4; (c) HPT1/2; (d) HPT1; (e) HPT2; (f) HPT5 ((e) and (f) contain hardness indentations); (g) HPT10 and

(h) HPT16 samples.

Fig.3 shows backscattered SEM images of the Mg alloy after HPT processing. It is clear that after 1 turn HPT processing, the networks of eutectic regions (appearing bright in the SEM images) at the grain boundaries of the 1/2 radius and peripheral regions become deformed, and after HPT for 5 turns more intense shear and deformation are observed in these eutectic regions. After HPT for 10 turns, part of the distorted network of eutectic phases at the half-radius region are fragmented into smaller segments, and only a few coarse eutectic networks remain, whilst at the periphery of the disk most of the eutectic network structure is broken into homogeneously distributed fine particles. Such a homogenous refined microstructure can also be observed near the half-radius and edge regions after HPT for 16 turns. As shown in Fig. 4(a), the second phases are broken up into dispersed particles of about 1~10 μm after HPT for 16 turns. According to the TEM bright field image and corresponding selected area electron diffraction (SAED) pattern shown in Fig. 4(b), these fragments have face-centered cubic (fcc) structure with a lattice constant of 0.723 nm, which can be identified as Mg_3RE type compound (fcc, D03 structure, a = 0.720 nm) [17, 26]. These observations show that the microstructure refinement initially develops at the edge (where the strain is highest), and then spreads to the centre of the disk, but the microstructure still remains non-uniform over the disk even after 16 turns, particularly in the immediate vicinity of the central area. This is mainly due to the dependency of strain on distance to the centre of the disk: accumulated strain introduced by HPT decreases from periphery to the centre of the disk (see [27, 28] and Discussion).

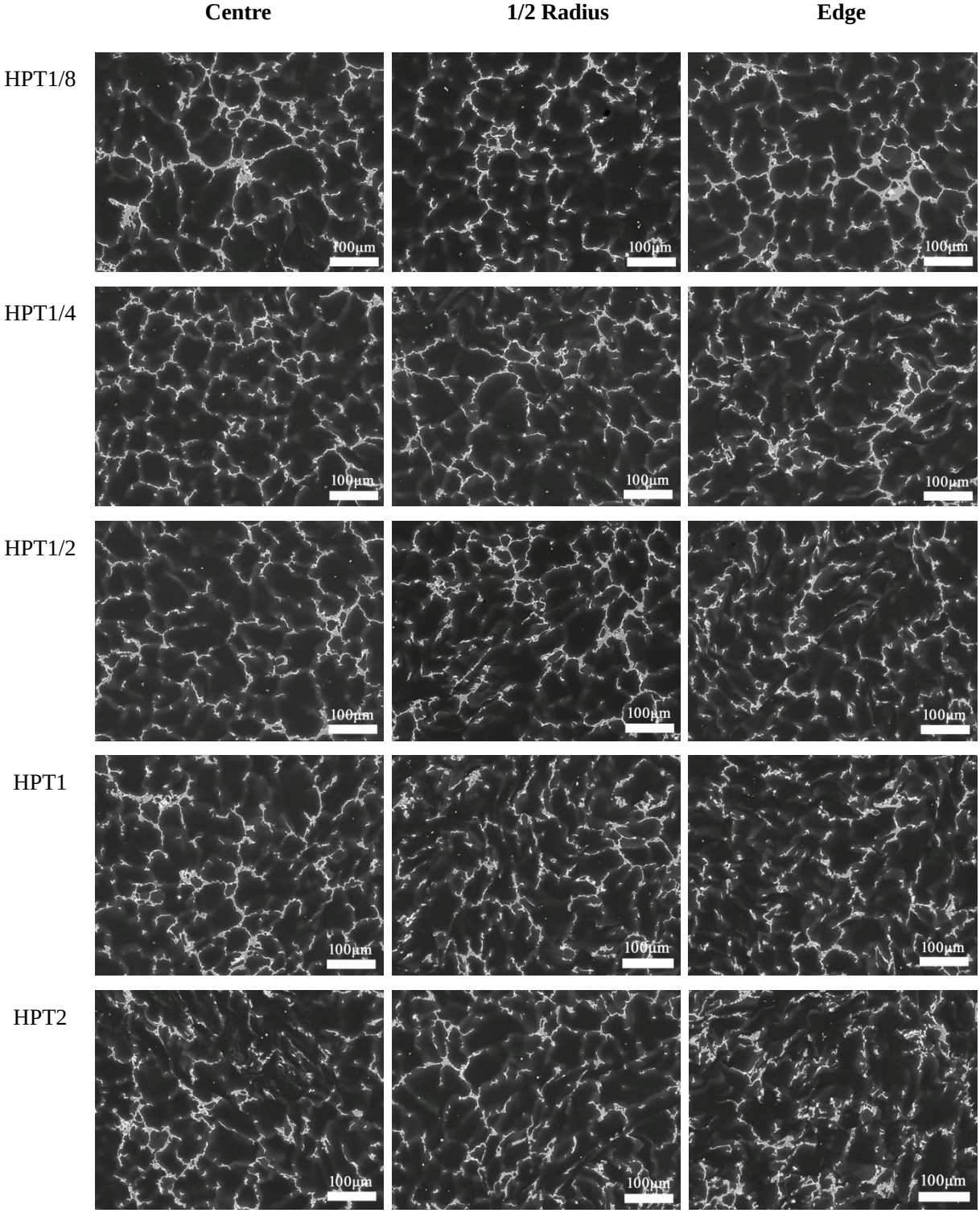
Centre
1/2 Radius
Edge
HPT1/8
HPT1/4
HPT1/2
HPT1
HPT2
100μm

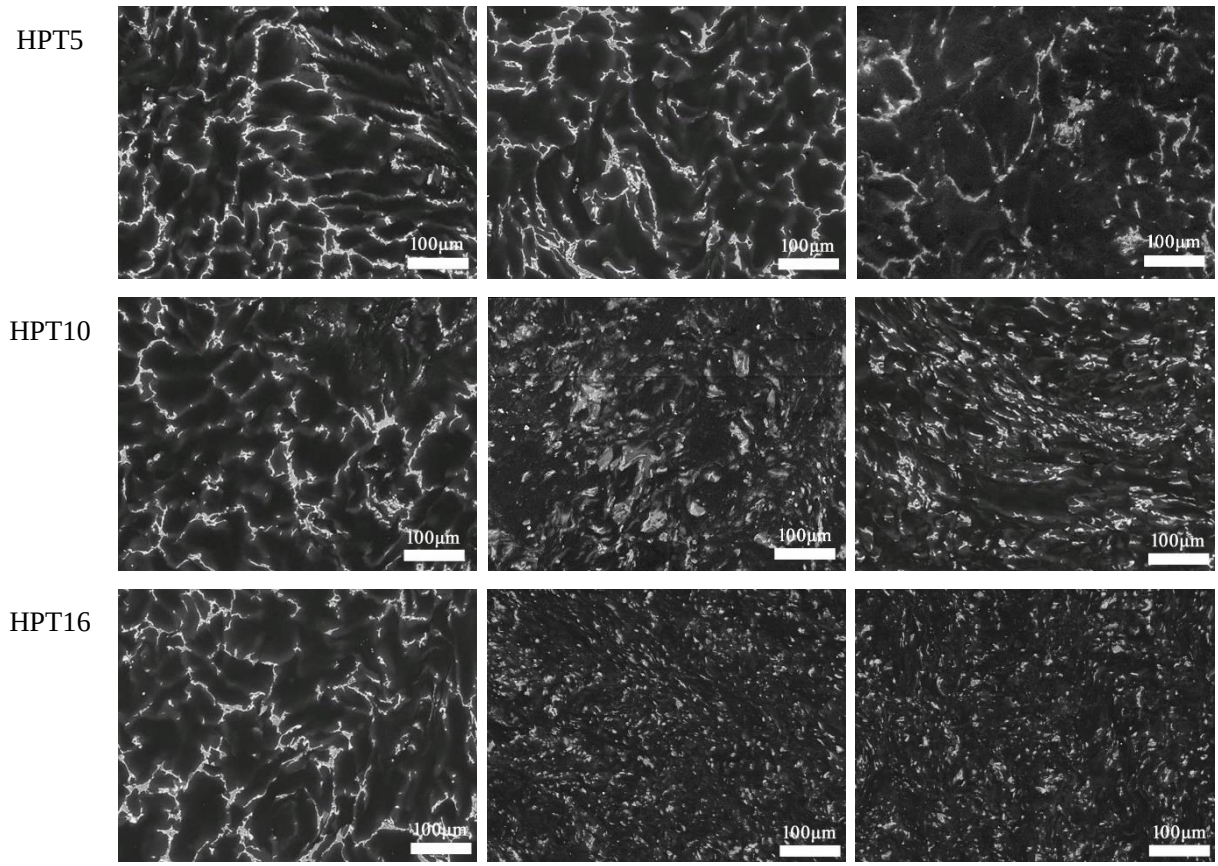

Fig.3 Backscattered electron SEM micrographs taken at positions close to the centre (left column), 1/2 radius (central column) and periphery (right column) on the polished surfaces of Mg-Gd-Y-Zn-Zr disks processed by HPT for various revolutions.

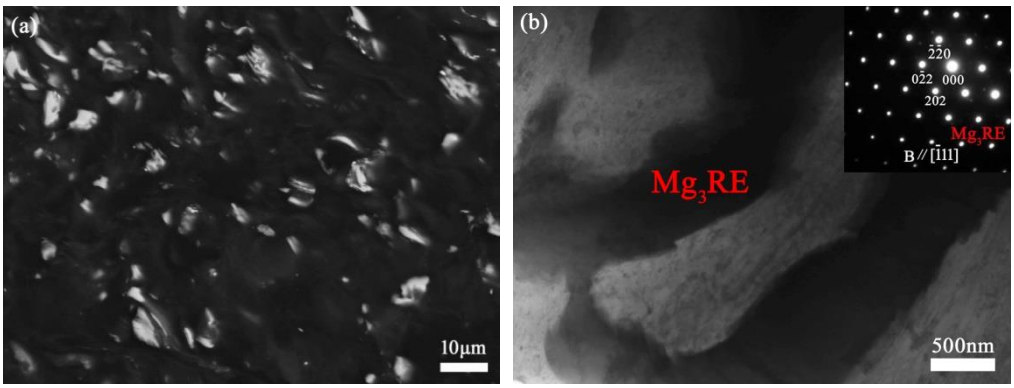

Fig.4 (a) Backscattered electron SEM image and (b) TEM image of broken-up $Mg_3(Gd,Y)$ phases at the half-radius region of samples processed by HPT for 16 turns, and inset is the SAED taken from the $Mg_3(Gd,Y)$ phase.

TEM images taken from the half-radius regions of the disks after HPT for different

numbers of turns are shown in Fig. 5. It can be seen that a high density of dislocation tangles and pile-ups are formed after HPT for 1/8 turn, and dislocation cell substructures appear in the alloy after HPT for 1/4 turn. After HPT processing by 1/2 turn, the SAED pattern shows elongated diffraction spots with short arcs (see Fig. 5(c)), indicating that subgrains with high internal stresses have developed. After HPT processing by 1 turn, TEM shows that dislocation cells and low-angle subgrains have evolved into nanocrystalline grains with average grain size of about 115 nm (see Fig. 5(d)), and the corresponding SAED pattern further supports this (inset in Fig. 5(d)). The non-uniform contrast observed in the grains is due to distortions of crystalline lattice caused by the large internal stresses [28]. With further increase of HPT turns, the grain structure is further refined. After HPT processing by 10 turns, an average grain size about 55 nm is obtained (Fig. 5(g)). After HPT for 16 turns, a more homogenous nanostructure with a grain size of ~55 nm is formed, as shown in Fig. 5(h) and (i), which is verified by the well-defined continuous rings of spots in the SAED pattern (Fig. 5(j)). Hence, after about 10 HPT turns grain refinement reaches saturation in the present Mg-Gd-Y-Zn-Zr alloy.

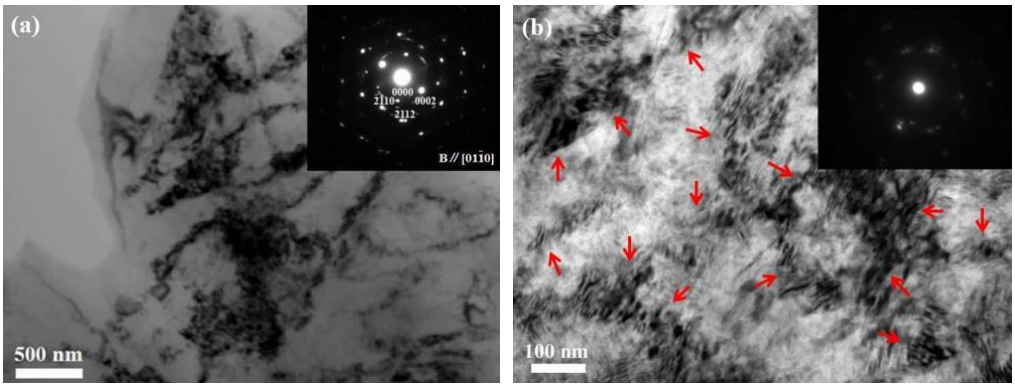

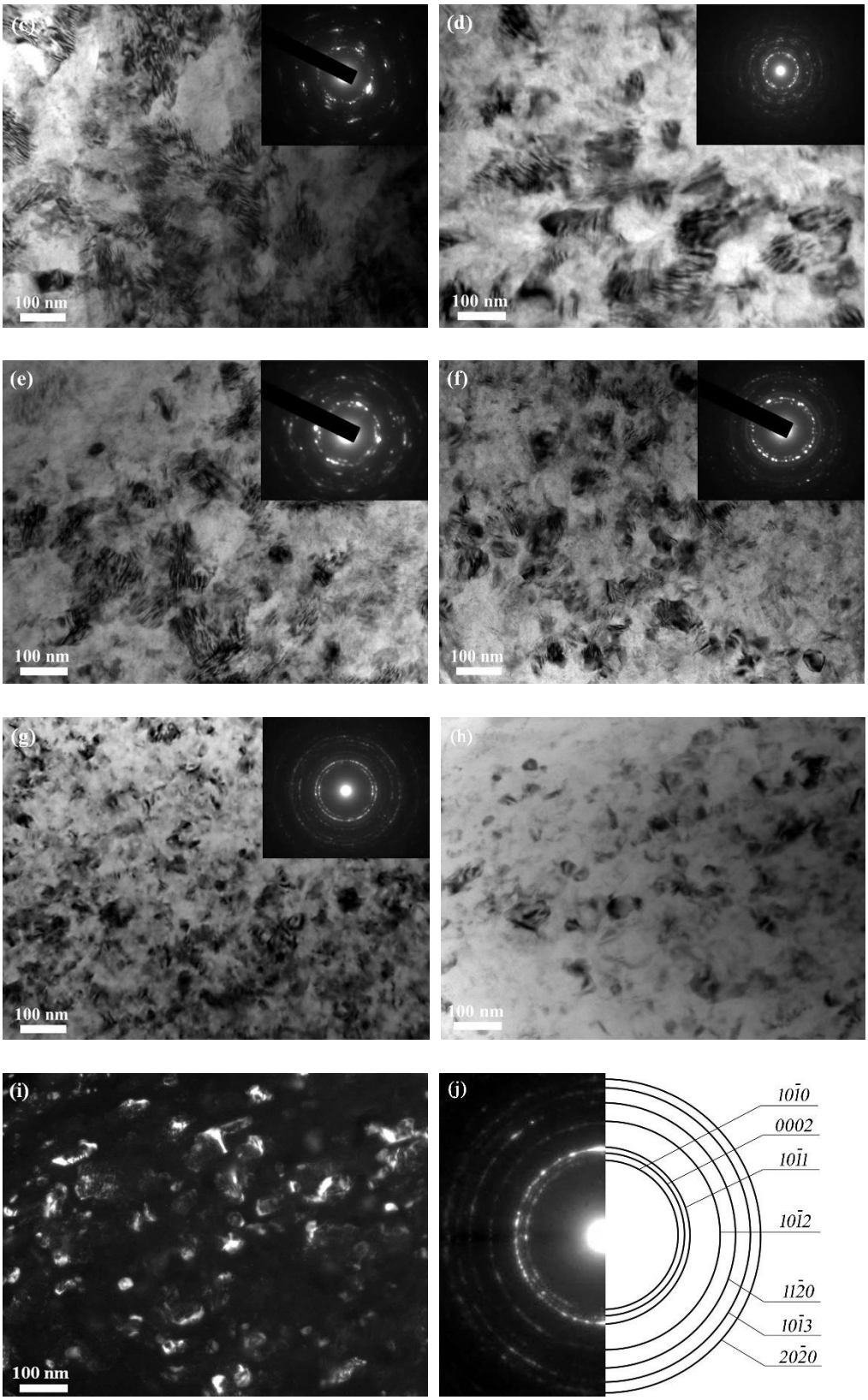

Fig.5 TEM bright field images and corresponding SAED patterns taken from the positions close to 1/2 radius of Mg-Gd-Y-Zn-Zr disks processed by HPT for various revolutions: (a) HPT1/8; (b)

HPT1/4; (c) HPT1/2; (d) HPT1; (e) HPT2; (f) HPT5; (g) HPT10; (h) HPT16; (i) dark field image of (h); (j) SAED pattern of (h).

3.2 XRD analysis of the HPT-processed samples

Fig. 6(a) shows XRD spectra of our Mg-8.2Gd-3.8Y-1.0Zn-0.4Zr alloy processed by HPT for different turns, and sections of the spectra between 30 and 41° are shown in Fig. 6(b). The XRD data show that the as-cast alloy is mainly composed of α-Mg and Mg_3RE phase, and after HPT processing, the diffraction peaks for these phases remain present and no additional peaks arise. As shown in Fig. 6(b), HPT processing induces a slight shift to lower angle (i.e. larger lattice parameter) for the α-Mg diffraction peaks whilst the intensities of the Mg_3RE diffraction peaks decrease. The latter indicates the amount of Mg_3RE reduces (see also [13] and [29]).

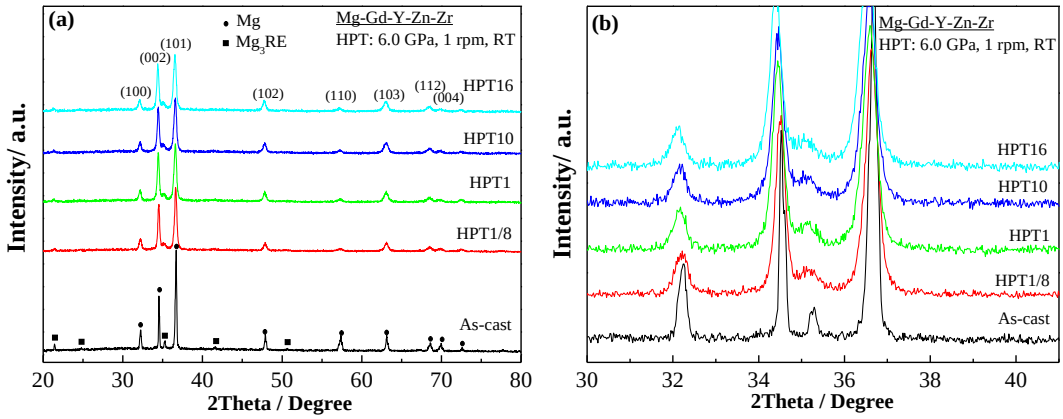

Fig.6 (a) Overview of XRD patterns of the as-cast and HPT-deformed Mg-Gd-Y-Zn-Zr with various revolutions; (b) enlarged section of the XRD patterns.

The dislocation densities, as obtained from the measured XRD microstrains using the Williamson-Smallman relationship [20-25], are plotted as a function of the number of HPT revolutions in Fig. 7. It can be seen that the dislocation density increases sharply at the early stage of HPT processing and then remains almost constant with further

plastic deformation, reaching a saturated value of around 3.2×10^{14} m^{-2} as a result of the dynamic equilibrium between dislocation generation and annihilation.

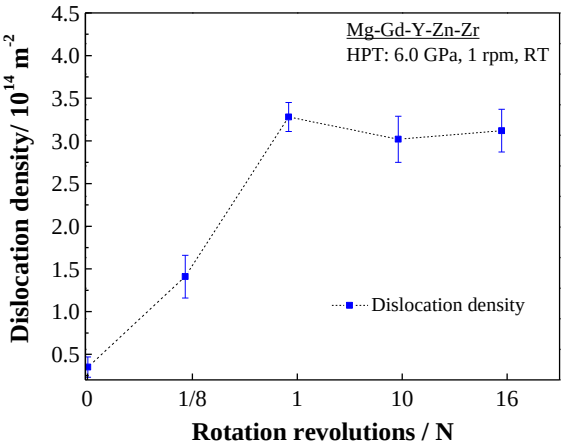

Fig. 7 The dislocation density plotted as a function of the number of HPT revolutions.

3.3 Microhardness evolution after HPT processing

The variations of the microhardness with respect to the distance from the disk centre after HPT for different revolutions is presented in Fig. 8. This figure shows that the microhardness of the alloy strongly increases as a result of HPT processing. As well as limited grain refinement (see section 3.1), the central region also exhibits much lower microhardness as compared to other regions of the disks, which is due to the very limited plastic deformation in the centre region [30], which is commonly found for a range of alloys processed by HPT. It also can be seen that the microhardness of the alloy increases with increasing HPT turns, although this hardening slows substantially as the number of turns passes 2 to 5 turns. With the exception of the softer narrow region around the centre of the sample, the hardness reaches ~115 HV after 16 turns. The microhardness variation along the diameter shows some scatter in the first several turns of HPT. The disk processed by HPT for 16 turns has similar microhardness as the disk processed by HPT for 10 turns.

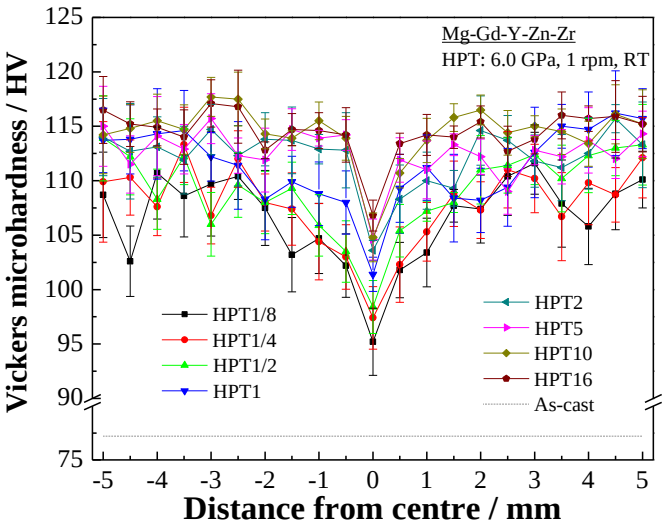

Fig.8 Variation of HV across the diameter of HPT-deformed Mg-Gd-Y-Zn-Zr disks with different revolutions. The dashed line indicates the Vickers microhardness of the as-cast alloy.

4. Discussion

Previous work has shown that when the cast Mg-8.2Gd-3.8Y-1.0Zn-0.4Zr (wt%) alloy that is studied in the present paper is extruded at 400 ^{o}C, a bimodal microstructure consisting of coarse non-recrystallized deformed grains and fine dynamic recrystallization with an average grain size of ~8 μm is developed. The hardness of this extruded alloy is about 98 HV [15], which is much lower than the hardness of 115 HV obtained by the present HPT processing at room temperature of the same alloy. In this section we will explore how the high dislocation density induced by HPT processing and the exceptional microstructure refinement of Mg-Gd-Y-Zn-Zr alloy to nanometer range contribute to the high hardness.

With increasing numbers of HPT revolutions, both microstructure and microhardness of Mg-Gd-Y-Zn-Zr alloy gradually reach a saturation state. Fig. 9 shows the variation of microhardness with the imposed equivalent strain. The equivalent strain ε_{eq} is expressed as [10, 31, 32]:

$$\varepsilon_{eq} = \frac{2}{\sqrt{3}} \ln\left[\left(1 + \frac{\gamma^2}{4}\right)^{1/2} + \frac{\gamma}{2}\right] \quad (2)$$

$$\gamma = \frac{2\pi r N}{h} \quad (3)$$

where γ is the shear strain, r is the radial distance from the disk centre, h is the thickness of the disk and N is the total number of rotations.

It can be seen in Fig.9 that the microhardness of our HPT-processed alloy increases strongly as equivalent strain increases from 0 to 2, and further straining causes progressively smaller increases in hardness with no detectable further hardening at strains in excess of 6. The saturation value of hardness is ~115 HV. In Fig.9 the hardness values are all in a narrow band, which indicates that the local strain in the various samples is the determining factor for the hardness. Although the theoretical strain calculated from Eq. 2 is zero at the centre, the centre area has also undergone a certain degree of effective plastic deformation after HPT processing because of the imposed high compressive pressure, whilst strain gradients at the centre [33] cause the generation of geometrically necessary dislocations which causes hardening.

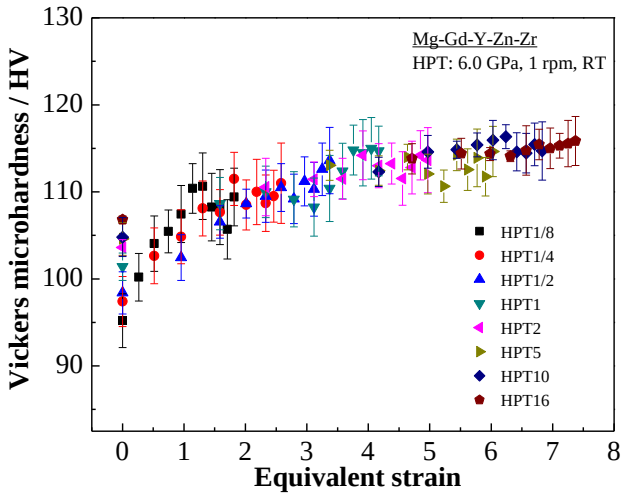

Fig. 9 Dependence of Vickers microhardness on the equivalent strain of HPT-deformed Mg-Gd-Y-Zn-Zr disks with different revolutions. The hardness of the alloy prior to HPT (i.e. in as-cast condition) is 77 HV.

The XRD data reveal a progressive increase in the lattice parameter of the α-Mg phase with increasing HPT deformation and decreasing intensity of the Mg_3RE peaks. As RE elements dissolved in the Mg-rich phase increase the lattice parameter [34], these observations clearly indicate that some dissolution of the Mg_3RE phase particles occurs. The driving force for such dissolution lies in the increase of free energy of the refined Mg_3RE phase caused by the increased Mg_3RE/α-Mg surface area (i.e. the Gibbs-Thomson effect). This increases the (metastable) solubility of the RE elements in the α-Mg phase. The increase in solute content of the α-Mg will cause some hardening. It is noted that for a Mg-1.8Gd-1Zn-0.1Zr (at%) alloy processed by ECAP at 375 °C， some of the β-Mg_5(Gd,Zn) phase was dissolved as a result of the severe shear deformation, with LPSO phase forming as a result of the dissolution of β phase [4]. However, in the present room temperature processing, the formation of LPSO structure is not observed, which may be due to diffusion rates being too low to allow the required redistribution of alloying elements at ambient temperature.

It has been reported that in HPT-processed AZ31 and AZ91 alloys the dislocation density, as measured by positron lifetime spectrometry and XRD, increased gradually to about ~1.2×10^{14} m^{-2} and ~2×10^{14} m^{-2}, respectively, after processing for the first several turns [35, 36], whilst the model in [37] predicts a dislocation density of 1.4×10^{14} m^{-2} for pure Mg processed by HPT to a saturated hardness. In the present alloy, the dislocation density increases dramatically at the early stage, and after 10 and 16 turns, the saturated dislocation density reaches ~3.2×10^{14} m^{-2}. The increased dislocation density for the present Mg-Gd-Y-Zn-Zr alloy is thought to be related to the combined

addition of Gd, Y and Zn elements which decreases the stacking fault energy (SFE) [38, 39]. Increased width of stacking faults makes dislocation cross-slip and climb more difficult, which makes dynamic recovery slow and difficult, leading to an increased dislocation density and high strain hardening effect in the first several HPT turns. In previous work on SPD processing of Mg alloys, often a solution treatment was conducted before SPD [11, 12, 40], whereas in this study HPT was performed on the as-cast Mg-Gd-Y-Zn-Zr alloy containing LPSO and $Mg_3(Gd,Y)$ phases. The dislocations will pile up at these second phases in grain interiors and at grain boundaries, i.e. they are effective barriers for blocking or pinning of dislocations. As a result, both the low SFE and second phase particles, which are gradually refined as HPT strain increases, appear to be responsible for the high dislocation density, which contributes to the high strain hardening and hardness improvement of our HPT processed Mg-Gd-Y-Zn-Zr alloy.

The contributions of dislocation hardening and grain size hardening can be analyzed with existing models [37], e.g. dislocation hardening is generally accepted to be given by

$$\Delta\tau_d = \alpha_1 Gb\sqrt{\rho} \quad (4)$$

where $\Delta\tau_d$ is the increment in critical resolved shear stress of the grain, ρ is the dislocation density in the grain, G is the shear modulus (17.7 GPa [37]), b is the length of the Burgers vector (taken as 0.3197 nm), α_1 is a constant equalling about 0.3. The ratio of critical resolves shear stress to yield strength is given by the Taylor factor. For the grain size strengthening, $\Delta\sigma_{GB}$, often the Hall-Petch relation is applied:

$$\Delta\sigma_{GB} = \frac{k_{HP}}{d_g^{1/2}} \quad (5)$$

where k_{HP} is the Hall-Petch constant (following the assessment in [37] it is taken as 40.7 MPa·μm$^{1/2}$), d_g is the grain size.

Using Eq. 4, the contribution of dislocation hardening for a dislocation density of 3.2×10^{14} m^{-2} (measured for the present alloy) to the yield strength of the Mg-rich matrix phase is ~68 MPa, which equates to a hardness increment of about 23 HV. Using Eq. 5, together with the assessment of k_{HP} in [37], the contribution of grain size hardening for a α-Mg phase with grain size of 55 nm (see section 3.1 and Fig. 5(h) and (i)) is ~51 HV. This assessment indicates that the combination of dislocation hardening and grain boundary hardening provides most of the hardening of the present HPT processed alloy, with the grain boundary hardening providing by far the strongest contribution. This explains the observation that whilst the dislocation density reaches saturation within 1 turn, the hardness continues to rise substantially on further deformation. Solution hardening of the α-Mg phase (promoted by the enhanced solubility of Gd and Y caused by the Gibbs-Thomson effect) and dispersion hardening (by the dispersed $Mg_3(Gd,Y)$ intermetallic particles) will provide further contributions to the strengthening.

It is also interesting to note that whereas for HPT-processed pure Mg the contributions of dislocation hardening and grain size hardening contribute about equally to the strength / hardness of the material [37], the above assessment based on Eqs. 4 and 5 indicates that for the present HPT processed Mg-Gd-Y-Zn-Zr alloy the grain size hardening contribution is stronger than dislocation hardening contribution by

a factor of ~2. This is related to the much enhanced grain refinement in the present alloy (down to 55 nm) as compared to the grain refinement achieved in pure Mg (typically down to 1 μm). Also for HPT processed conventional Mg alloys such as AZ31 (grain size typically refined down to 1 or 0.5 μm, depending on conditions [41]), AZ61 (grain size typically refined down to 0.2 μm [27]) and ZK60 (grain size typically refined down to 1 μm [42]), the grain refinement is more limited and grain size strengthening will be substantially less than for the present HPT processed Mg-Gd-Y-Zn-Zr alloy. Apparently the combination of the present alloying (Gd, Y, Zn and Zr) and the stabilization of the grain structure against grain growth and recovery by virtue of the dense homogeneous dispersion of fine intermetallic particles is particularly effective in producing grain refinement. Thus, compared to pure Mg and several other Mg alloys, the present alloy with high RE content shows an unusually strong refinement of grain structure which provides the main strengthening mechanism in HPT processed condition.

When the equivalent strain induced by HPT increases beyond ~6.0, the grain size as well as the hardness of the Mg-Gd-Y-Zn-Zr alloy reach saturation level. The occurrence of such saturation of grain size is thought to be due to the microstructure becoming saturated with lattice defects, primarily in the form of vacancies and dislocations, causing additional plastic deformation to produce dynamic recovery in which the work of mechanical deformation is effectively transformed into heat rather than additional lattice defects [7, 37]. It is well known that grain boundaries can act as dislocation sinks [9, 37] and when the grains are refined to nano size at equivalent

strains above ~6.0, a balance is established between generation of dislocations by HPT and absorption of dislocations at grain boundaries. As a result, the hardness reaches a saturation state.

Therefore, the significant increase of microhardness of HPT-processed Mg-Gd-Y-Zn-Zr alloy compared to the extruded alloy is ascribed to the nano-sized grains, high dislocation density and fine dispersed $Mg_3(Gd,Y)$ fragments, all caused by the high equivalent strains introduced by HPT and aided by the alloying.

5. Conclusions

The as-cast Mg-8.2Gd-3.8Y-1.0Zn-0.4Zr alloy was subjected to high pressure torsion (HPT) at ambient temperature under 6 GPa from 1/8 to 16 turns, and the influences of imposed strain on both microstructure and mechanical properties were evaluated. The following conclusions are drawn：

(1) The grain size of the as-cast Mg-Gd-Y-Zn-Zr alloy is significantly refined with increasing HPT turns. When equivalent strain is increased to ~6.0, a homogeneous grain structure with grain size of about 55 nm is obtained in the alloy, and the grain size remains constant with further HPT deformation. The dislocation density introduced by HPT processing exceeds that of HPT processed AZ31 and AZ91 Mg-Al-Zn conventional alloys. Dislocation cells and low-angle subgrain boundaries are formed during the initial stages of HPT, and then gradually transform into high-angle grain boundaries at high strains.

(2) Due to the high strains caused by HPT, the initial coarse netlike $Mg_3(Gd,Y)$ second phase structures present in the as-cast state are effectively broken into small

particles with sizes of 1-10 μm, and are homogeneously dispersed in the matrix after HPT for 16 turns.

(3) The microhardness of the Mg-Gd-Y-Zn-Zr alloy is increased significantly after HPT processing, and a saturated maximum value of 115 HV is obtained after 10 turns which is substantially higher than an extrusion of the same alloy. The improvement of microhardness is attributed primarily to the refined Mg grains in nanometer range, the high dislocation density induced by HPT processing and homogeneously dispersed small fine $Mg_3(Gd,Y)$ second phases.

Acknowledgement

This work was supported by National Nature Science Foundation of China (No.51571067) and National Key Research and Development Program of China (No. 2016YFB0301102).

References

[1] B.L. Mordike, T. Ebert, Magnesium: properties-applications-potential, Mater. Sci. Eng. A 302 (2001) 37-45.

[2] Y. Kawamura, K. Hayashi, A. Inoue, Rapidly solidified powder metallurgy Mg97Zn1Y2 alloys with excellent tensile yield strength above 600 MPa, Mater. Trans. 42 (2001) 1172-1176.

[3] Q. Yang, B.L. Xiao, D. Wang, M.Y. Zheng, K. Wu, Z.Y. Ma, Formation of long-period stacking ordered phase only within grains in Mg-Gd-Y-Zn-Zr casting by friction stir processing, J. Alloys Compd. 581 (2013) 585-589.

[4] F.M. Lu, A.B. Ma, J.H. Jiang, D.H. Yang, Y.C. Yuan, L.Y. Zhang, Formation of profuse long period stacking ordered microcells in Mg-Gd-Zn-Zr alloy during multipass ECAP process, J. Alloys Compd. 601 (2014) 140-145.

[5] A.B. Ma, J.H. Jiang, N. Saito, I. Shigematsu, Y.C. Yuan, D.H. Yang, Y. Nishida, Improving both strength and ductility of a Mg alloy through a large number of ECAP passes, Mater. Sci. Eng. A 513-514 (2009) 122-127.

[6] R. Lapovok, X. Gao, J.F. Nie, Y. Estrin, S.N. Mathaudhu, Enhancement of properties in cast Mg-Y-Zn rod processed by severe plastic deformation, Mater. Sci. Eng. A 615 (2014) 198-207.

[7] A.P. Zhilyaev, T.G. Langdon, Using high-pressure torsion for metal processing: fundamentals and application, Prog. Mater. Sci. 53 (2008) 893-979.

[8] Y. Huang, R.B. Figueiredo, T. Baudin, F. Brisset, T.G. Langdon, Evolution of strength and

homogeneity in a magnesium AZ31 alloy processed by high-pressure torsion at different temperatures, Adv. Eng. Mater. 14 (2012) 1018-1026.
[9] L.S. Toth, C.F. Gu, Ultrafine-grain metals by severe plastic deformation, Mater. Charact. 92 (2014) 1-14.
[10] X.G. Qiao, Y.W. Zhao, W.M. Gan, Y. Chen, M.Y. Zheng, K. Wu, N. Gao, M.J. Starink, Hardening mechanism of commercially pure Mg processed by high pressure torsion at room temperature, Mater. Sci. Eng. A 619 (2014) 95-106.
[11] O.B. Kulyasova, R.K. Islamgaliev, Y.H. Zhao, R.Z. Valiev, Enhancement of the mechanical properties of an Mg-Zn-Ca alloy using high-pressure torsion, Adv. Eng. Mater. 17 (2015) 1738-1741.
[12] J. Čížek, I. Procházka, B. Smola, I. Stulíková, R. Kužel, Z. Matěj, V. Cherkaska, R.K. Islamgaliev, O. Kulyasova, Microstructure and thermal stability of ultrafine grained Mg-based alloys prepared by high-pressure torsion, Mater. Sci. Eng. A 462 (2007) 121-126.
[13] R. Alizadeh, R. Mahmudi, A.H.W. Ngan, Y. Huang, T.G. Langdon, Superplasticity of a nano-grained Mg-Gd-Y-Zr alloy processed by high-pressure torsion, Mater. Sci. Eng. A 651 (2016) 786-794.
[14] S.V. Dobatkin, L.L. Rokhlin, E.A. Lukyanova, M.Y. Murashkin, T.V. Dobatkina, N.Y. Tabachkova, Structure and mechanical properties of the Mg-Y-Gd-Zr alloy after high pressure torsion, Mater. Sci. Eng. A 667 (2016) 217-223.
[15] Y.Q. Chi, M.Y. Zheng, C. Xu, Y.Z. Du, X.G. Qiao, K. Wu, X.D. Liu, G.J. Wang, X.Y. Lv, Effect of ageing treatment on the microstructure, texture and mechanical properties of extruded Mg-8.2Gd-3.8Y-1Zn-0.4Zr (wt%) alloy, Mater. Sci. Eng. A 565 (2013) 112-117.
[16] C. Xu, M.Y. Zheng, S.W. Xu, K. Wu, E.D. Wang, S. Kamado, G.J. Wang, X.Y. Lv, Microstructure and mechanical properties of Mg-Gd-Y-Zn-Zr alloy sheets processed by extrusion, hot rolling and ageing, Mater. Sci. Eng. A 559 (2013) 844-851.
[17] C. Xu, M.Y. Zheng, Y.Q. Chi, X.J. Chen, K. Wu, E.D. Wang, G.H. Fan, P. Yang, G.J. Wang, X.Y. Lv, S.W. Xu, S. Kamado, Microstructure and mechanical properties of the Mg-Gd-Y-Zn-Zr alloy fabricated by semi-continuous casting, Mater. Sci. Eng. A 549 (2012) 128-135.
[18] M.J. Starink, X.G. Qiao, J. Zhang, N. Gao, Predicting grain refinement by cold severe plastic deformation in alloys using volume averaged dislocation generation, Acta Mater. 57 (2009) 5796-5811.
[19] A. Thorvaldsen, The intercept method-1. Evaluation of grain shape, Acta Mater. 45 (1997) 587-594.
[20] Y. Chen, N. Gao, G. Sha, S.P. Ringer, M.J. Starink, Microstructural evolution, strengthening and thermal stability of an ultrafine-grained Al-Cu-Mg alloy, Acta Mater. 109 (2016) 202-212.
[21] M. Ferrari, L. Lutterotti, Method for the simultaneous determination of anisotropic residual stresses and texture by X-ray diffraction, J. Appl. Phys. 76 (1994) 7246-7255.
[22] L. Lutterotti, S. Gialanella, X-ray diffraction characterization of heavily deformed metallic specimens, Acta Mater. 46 (1998) 101-110.
[23] Y. Chen, N. Gao, G. Sha, S.P. Ringer, M.J. Starink, Strengthening of an Al-Cu-Mg alloy processed by high-pressure torsion due to clusters, defects and defect-cluster complexes, Mater. Sci. Eng. A 627 (2015) 10-20.
[24] G.K. Williamson, R.E. Smallman, Dislocation densities in some annealed and cold-worked metals from measurements on the X-Ray debye-scherrer spectrum, Philos. Mag. 1 (1956) 34-46.
[25] Y.H. Zhao, X.Z. Liao, Z. Jin, R.Z. Valiev, Y.T. Zhu, Microstructures and mechanical properties of ultrafine grained 7075 Al alloy processed by ECAP and their evolutions during annealing, Acta Mater. 52 (2004) 4589-4599.

[26] M. Yamasaki, M. Sasaki, M. Nishijima, K. Hiraga, Y. Kawamura, Formation of 14H long period stacking ordered structure and profuse stacking faults in Mg-Zn-Gd alloys during isothermal aging at high temperature, Acta Mater. 55 (2007) 6798-6805.
[27] Y. Harai, M. Kai, K. Kaneko, Z. Horita, T.G. Langdon, Microstructural and mechanical characteristics of AZ61 magnesium alloy processed by high-pressure torsion, Mater. Trans. 49 (2008) 76-83.
[28] Y. Estrin, A. Molotnikov, C.H.J. Davies, R. Lapovok, Strain gradient plasticity modelling of high-pressure torsion, J. Mech. Phys. Solids 56 (2008) 1186-1202.
[29] R. Alizadeh, R. Mahmudi, A.H.W. Ngan, T.G. Langdon, Microstructural stability and grain growth kinetics in an extruded fine-grained Mg-Gd-Y-Zr alloy, J. Mater. Sci. 50 (2015) 4940-4951.
[30] J. Crump, X.G. Qiao, M.J. Starink, The effect of high-pressure torsion on the behaviour of intermetallic particles present in Al-1Mg and Al-3Mg, J. Mater. Sci. 47 (2012) 1751-1757.
[31] J. Zhang, M.J. Starink, N. Gao, Microstructure development and hardening during high pressure torsion of commercially pure aluminium: Strain reversal experiments and a dislocation based model, Mater. Sci. Eng. A 528 (2011) 2581-2591.
[32] I. Saunders, J. Nutting, Deformation of metals to high strains using combination of torsion and compression, Met. Sci. 18 (1984) 571-575.
[33] H.J. Lee, B. Ahn, M. Kawasaki, T.G. Langdon, Evolution in hardness and microstructure of ZK60A magnesium alloy processed by high-pressure torsion, J. Mater. Res. Technol. 4 (2015) 18-25.
[34] Y.R. Wu, W.Y. Hu, Comparison of the solid solution properties of Mg-RE (Gd, Dy, Y) alloys with atomistic simulation, Res. Lett. Phys. 2008 (2008) 1-4.
[35] J. Vrátná, M. Janeček, J. Čížek, D.J. Lee, E.Y. Yoon, H.S. Kim, Mechanical properties and microstructure evolution in ultrafine grained AZ31 alloy processed by severe plastic deformation, J. Mater. Sci. 48 (2013) 4705-4712.
[36] A.S.J. Al-Zubaydi, A.P. Zhilyaev, S.C. Wang, P. Kucita, P.A.S. Reed, Evolution of microstructure in AZ91 alloy processed by high-pressure torsion, J. Mater. Sci. 51 (2016) 3380-3389.
[37] M.J. Starink, X. Cheng, S. Yang, Hardening of pure metals by high-pressure torsion: A physically based model employing volume-averaged defect evolutions, Acta Mater. 61 (2013) 183-192.
[38] B. Smola, I. Stulikova, J. Pelcova, B.L. Mordike, Significance of stable and metastable phases in high temperature creep resistant magnesium-rare earth base alloys, J. Alloys Compd. 378 (2004) 196-201.
[39] M. Suzuki, T. Kimura, J. Koike, K. Maruyama, Effects of zinc on creep strength and deformation substructures in Mg-Y alloy, Mater. Sci. Eng. A 387-389 (2004) 706-709.
[40] F.Q. Meng, J.M. Rosalie, A. Singh, H. Somekawa, K. Tsuchiya, Ultrafine grain formation in Mg-Zn alloy by in situ precipitation during high-pressure torsion, Scr. Mater. 78-79 (2014) 57-60.
[41] L.R.C. Malheiros, R.B. Figueiredo, T.G. Langdon, Grain size and microhardness evolution during annealing of a magnesium alloy processed by high-pressure torsion, J. Mater. Res. Technol. 4 (2015) 14-17.
[42] S.A. Torbati-Sarraf, T.G. Langdon, Properties of a ZK60 magnesium alloy processed by high-pressure torsion, J. Alloys Compd. 613 (2014) 357-363.